THE JOURNAL OF PHYSICAL CHEMISTRY C

Article

pubs.acs.org/JPCC

Ionic Liquid Aqueous Solutions under Nanoconfinement

Javier Rodriguez,[†,‡] M. Dolores Elola,[†] and D. Laria*[,†,§]

[†]Departamento de Física de la Materia Condensada, Comisión Nacional de Energía Atómica, Avenida Libertador 8250, 1429 Buenos Aires, Argentina

[‡]ECyT, UNSAM, Martín de Irigoyen 3100, 1650, San Martín, Provincia de Buenos Aires, Argentina

[§]Departamento de Química Inorgánica Analítica y Química-Física e INQUIMAE, Facultad de Ciencias Exactas y Naturales, Universidad de Buenos Aires, Ciudad Universitaria, Pabellón II, 1428 Buenos Aires, Argentina

ABSTRACT: We extend our previous molecular dynamics analysis of confined aqueous electrolytes within cylindrical hydrophobic pores of nanometric dimensions [Videla et al. *J. Chem. Phys.* **2011**, *135*, 104503] to the case of room temperature ionic liquid (RTIL) solutions, with concentrations close to $c \sim 1$ M. Equilibrium and dynamical characteristics of two imidazolium-based RTILs, differing in the hydrophobicity of the corresponding anionic species, were considered. The solutions within the pore were modeled in contact with "bulk-like" reservoirs, which served as reference systems to gauge the magnitude of the modifications observed in the global densities and in the transport coefficients. The density fields associated to the ionic species present a marked enhancement near the pore walls; this leads to increments of the global RTIL concentration within the pores, which are intermediate between 2 and 3 times the ones observed in the bulk reservoirs. These modifications are more marked in solutions containing more hydrophobic anionic species. In both cases, selective adsorption of imidazolium groups at the pore walls prevails; these wall-solvation states are characterized by a parallel orientation of the imidazolium ring, with respect to the pore surface. Mass and charge transport were also investigated. The segregation of the ionic species towards the pore wall promotes a sharp drop in the individual ionic diffusion coefficients. Nonuniform trends in the modifications of the ionic conductivity were found. Our results show that charge transport is the result of a complex interplay between competing effects involving modifications in the local concentrations, retardations in the ionic mobility, and dynamical cross-correlations, as well. A physical interpretation of the latter effects is provided in terms of the differences in the spatial correlations of the ionic species within the interior of the pore.

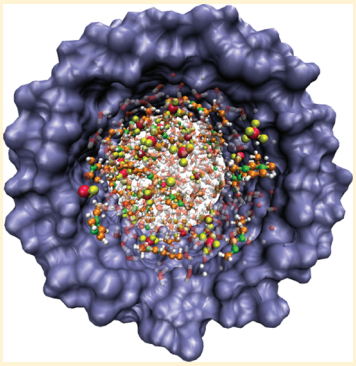

I. INTRODUCTION

Room temperature ionic liquids (RTILs) are molten salts that combine organic cations—such as alkyl-substituted imidazolium, pyridinimum, or phosphonium groups—and organic or inorganic anions ranging from simple ionic species (e.g., Cl^-, Br^-) up to more bulky and hydrophobic moieties, like BF_4^- or PF_6^-. Compared to classical organic solvents, these liquids exhibit several appealing physicochemical properties that make them suitable to host reactive processes in an "environmentally friendly" fashion. The list includes: low melting point, low volatility and flammability, high chemical and thermal stability, and high polarity, to cite a few relevant characteristics.

The incorporation of water to ionic liquids leads to a wide variety of new phases determined, to a large extent, by the range of miscibility of each particular salt. In the vast majority of cases, the miscibility is controlled by the corresponding anion.[1] From a microscopic perspective, the structure of these ionic phases is far from being simple.[2−7] In many cases, the amphiphilic nature of the cationic species leads to spatial heterogeneities at the mesoscopic level involving clustering[8−10] and self-organization phenomena.[11−16] Aqueous solutions of ILs present a series of practical applications in a variety of areas such as extraction processes in analytical chemistry,[17,18] synthetic routes,[19] and cooling cycles.[20]

The presence of a macroscopic solid/liquid or gas/liquid interface brings more complexities in the microscopic scenario. Most notable are those associated with local concentration fluctuations[21−24] and enhancement of orientational correlations involving different molecular groups at the vicinity of the interfaces.[25−27] These modifications, in turn, also have important consequences in the dynamical behavior of the different species[28,29] and may give rise to interesting catalytic applications.[30,31]

It is also of interest to examine how the resulting structures of these binary solutions can be even further modified when they are confined within pores or slits,[32,33] with nanometric linear dimensions. For example, using a combination of differential scanning calorimetry and spectroscopic measurements, Sing et al.[34] detected changes in phase equilibria of imidazolium-based ionic liquids confined in a silica gel matrix with nanometric dimensions. In addition, Coasne et al.[35] have examined the structure and dynamics of RTILs, tightly bound to the walls of silica pores at different filling conditions. Iacob and collaborators have reported results from dielectric spectroscopy and magnetic resonance experiments that reveal

Received: November 17, 2011
Revised: January 25, 2012
Published: January 27, 2012

up to 10-fold reductions in the diffusion coefficients of ionic liquids in oxidized nanoporous silica membranes.[36]

Yet, the information about microscopic characteristics of confined water−RTIL solutions is still very scarce. To gain physical insight about the subject, we undertook a series of molecular dynamics experiments involving aqueous solutions of two imidazolium-based RTILs, confined within cylindrical hydrophobic pores with radius close to 1 nm. To clearly identify the modifications introduced by the confinement, the solution within the pore was brought into contact with a reference, "bulk-like" reservoir. In a broader context, the present work extends a recent analysis[37] that we performed, in which we examined aqueous NaCl solutions within similar pores. Although these two systems could be cast within the same conceptual framework, this new set of simulation results reveals that the structural and dynamical features of the confined RTIL solutions differ from those observed in simpler aqueous electrolytes at a qualitative level.

The organization of the paper is as follows: in Section II, we briefly describe the model and technical details of the simulation procedure. Equilibrium and time-dependent characteristics of confined RTIL solutions are presented in Section III. The last section includes a summary of the main conclusions of the present work.

II. MODEL

The systems under investigation were similar to the ones examined in our earlier work, so the description here will be restricted to their main features. A more detailed presentation can be found in ref 37. We considered a model cylindrical pore of length l = 33 Å and radius R = 12.5 Å, in contact with reservoirs containing RTIL solutions, with a global concentration close to $c \sim 1$ M. The pore was placed at the central part of a fully periodic system, with its longitudinal axis aligned along the z-axis. The boxlengths of the simulation box were set to $L_x = L_y$ = 51 Å and $L_z \sim 87$ Å (see Figure 1). Two different

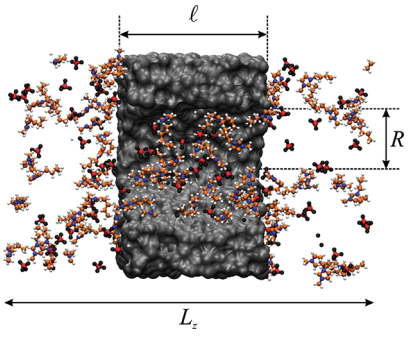

Figure 1. Snapshot of the model system comprising the central pore and the lateral bulk reservoir. For clarity purposes, water molecules have been removed.

solutions, differing in the "hydrophobic" characteristics of their corresponding anions, were considered: (i) 1-butyl-3-methylimidazolium chloride $[BMIM]^+[Cl]^-$ and (ii) 1-butyl-3-methylimidazolium tetrafluoroborate $[BMIM]^+[BF_4]^-$, hereafter referred to as IL1 and IL2, respectively.

The pore was constructed from a fused, silica-like, rectangular block with linear dimensions $L_x = L_y$ = 51 Å and L_z = 33 Å, previously equilibrated at T = 8000 K for about 1 ns. During this initial stage, all particles contained within a cylindrical section along the z-axis, of radius R = 12.5 Å, remained immobile.[38,39] The silica sample was then quenched down to ambient conditions, and the central resist was removed. The resulting structure presented dynamical characteristics similar to an amorphous solid phase.

The bored block was brought adjacent to previously equilibrated samples of RTIL aqueous solutions, which were allowed to permeate through the pore. The liquid phases of IL1 (IL2) comprised N_w = 4172 (4123) water molecules and N_{IL} = 102 (130) ion pairs. To facilitate the initial pore filling, the temperature was raised up to T = 473 K for about 5 ns and was slowly brought down to T = 323 K, until the global density of the solutions remained practically unchanged. During this last stage, the length of the simulation box along the z-axis was modified to bring the local water and salt concentrations in the $z \sim \pm L_z/2$, "bulk region", in reasonable agreement with experimental information. With this procedure, we could adjust the bulk salt concentrations to $c^{blk}_{IL1} \sim 0.87$ M and $c^{blk}_{IL2} \sim 0.77$ M and local water molar fractions to x^{blk}_{IL1} = 0.98 and x^{blk}_{IL2} = 0.98. The latter values coincide reasonably well with the data reported in refs 40 and 41.

Dynamical trajectories were generated using the NAMD package[42] and corresponded to microcanonical runs. In most cases, very long runs—involving, typically, five statistically independent trajectories, each one lasting ∼20 ns—were required, to obtain reasonable statistical averages. Concerning Hamiltonian details, the total energy was assumed to be pair decomposable. For water, we adopted the well-tested SPC/E model.[43] Solute species were modeled as fully flexible molecules, with intermolecular site−site interactions involving Lennard-Jones and Coulomb contributions. Inter- and intramolecular parameters were taken from ref 44. To reduce computational costs and be able to collect statistics along sufficiently long simulation runs, effects from polarization fluctuations were neglected. This is a delicate issue since it has been reported[45,46] that such approximations sometimes may lead to poor estimates, especially for dynamical properties. In addition to the explicit incorporation of dipole−dipole interactions, several modifications in the potential parameters, including the scaling of the site charges, have been recently proposed to improve simulation predictions.[47] Despite these drawbacks, we will show in the next section that our nonpolarizable Hamiltonian still provides reasonable estimates for diffusion constants of the water−IL solutions that we will examine. Interactions between pore sites and the rest of the fluid phase were of the Lennard-Jones type, exclusively. Details about the parameters can be found in our previous work.[37] The usual arithmetical and geometrical means were adopted to model length and energy cross interaction parameters. Ewald sums were implemented to handle the long-range nature of Coulomb interactions.[48]

III. RESULTS

A. Equilibrium Solvation Structures. The starting point of our analysis will be the consideration of different density fields along the z-direction, namely

$$\rho^z_\alpha(z) = \frac{1}{L_x L_y} \sum_i \langle \delta(z^i_\alpha - z) \rangle \tag{1}$$

where $(x^i_\alpha, y^i_\alpha, z^i_\alpha)$ corresponds to the coordinates of the center of mass of the ith particle of species (α = W, $[BMIM]^+$, $[Cl]^-$, $[BF_4]^-$) with respect to a coordinate system centered at the center of mass of the pore and $\langle ... \rangle$ denotes an equilibrium

dx.doi.org/10.1021/jp211101a | J. Phys. Chem. C 2012, 116, 5394−5400

ensemble average. Results for the different $\rho_\alpha^z(z)$ normalized by the corresponding bulk values, $\rho_\alpha^{blk} = \rho_\alpha^z(L_z/2)$, are shown in the top panels of Figures 2 and 3, for IL1 and IL2 solutions, respectively.

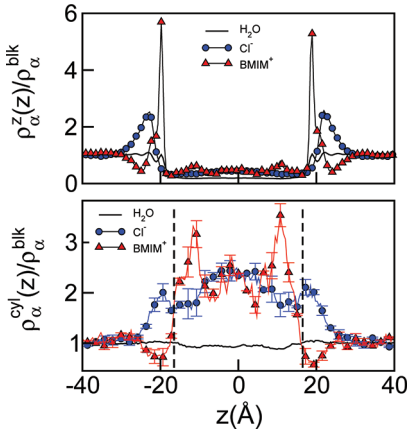

Figure 2. Top panel: Normalized density fields along the z-axis for confined $[BMIM]^+[Cl]^-$ aqueous solutions with $c_{IL1}^{blk} = 0.87$ M and $T = 323$ K. Bottom panel: Same as the top panel, for a restricted sampling along a central cylinder volume of radius R (see text). The error bars correspond to standard deviations obtained from five statistically independent, 20 ns trajectories (see text). The vertical dashed lines denote the pore boundaries.

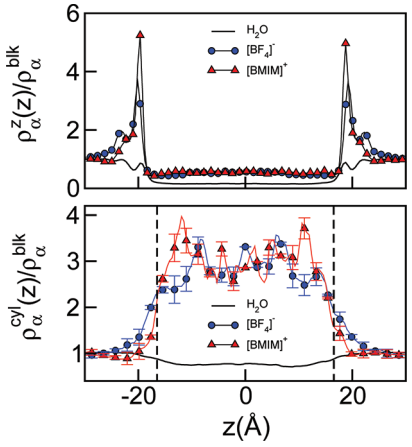

Figure 3. Same as Figure 2 for confined $[BMIM]^+[BF_4]^-$ aqueous solutions with $c_{IL2}^{blk} = 0.78$ M and $T = 323$ K.

The most prominent density fluctuations in the top panels correspond to cationic densities which show two peaks at $z \sim \pm 19$ Å, revealing a ~5-fold increment of the local densities with respect to the corresponding bulk values. The positions and magnitudes of these peaks suggest a tight adsorption of $[BMIM]^+$ groups, at the lateral walls of the solid slab which are in contact with the bulk solutions. The profiles for the anionic species show much broader and smaller peaks located at $z \sim \pm 22$ Å for $[Cl]^-$ and a doubly picked structure for $[BF_4]^-$ groups, shifted ~1 Å with respect to the positions of the $[BMIM]^+$ maxima, away from the walls and into the liquid phase.

As such, the profiles of $\rho_\alpha^z(z)$ inside the pore depend on the linear dimensions L_x and L_y of the simulation box. To get rid of that dependence, more insightful information about the characteristics of the densities can be gained, if one restricts the sampling to a cylindrical volume of radius similar to the pore one, namely

$$\rho_\alpha^{cyl}(z) = \frac{1}{\pi R^2} \sum_i \langle \delta(z_\alpha^i - z) \rangle_R \quad (2)$$

where $\langle ... \rangle_R$ denotes a statistical sampling restricted to those molecules whose distances to the z-axis are less than R.

Results for $\rho_\alpha^{cyl}(z)$ are depicted in the bottom panels of Figures 2 and 3. Compared to bulk results at $z \sim \pm L/2$, in both RTIL solutions, the water content within the pores decreases ~10−20%, whereas salt concentrations show clear enhancements, somewhat more marked in the IL2 case. Average values of the ionic densities computed along the $|z| < 16.5$ Å interval yield global concentrations within the pores close to $c_{IL1}^{pore} \sim 2.1$ M and $c_{IL2}^{pore} \sim 2.8$ M and water molar fractions $x_{IL1}^{pore} = 0.96$ and $x_{IL2}^{pore} = 0.93$. We remark that these features contrast sharply with the ones observed for confined aqueous solutions of NaCl, where the global salt concentrations within hydrophobic pores were found to be smaller than the values observed in the bulk.[37]

A close inspection of the two sets of plots presented in Figures 2 and 3 reveals important fluctuations of the ionic local densities, not only at the vicinity of the lateral wall of the bock but also at the pore rims. The case of IL1 solutions is perhaps the most evident: note that in the bottom panel of Figure 2 the $[BMIM]^+$ profile presents two minima at ~±20 Å, where the normalized density drops down to 0.8; moreover, as we move toward the interior of the pore, these two minima are followed by two maxima close to 3.5, at $z \sim \pm 15$ Å. Given the linear dimensions of the pore, we tend to believe that predictions for the confined liquid phase based on results obtained from these coupled pore−bulk systems will be affected by finite size effects to a non-negligible extent.

As a simple alternative to minimize these effects, and to move forward in our analysis of structural characteristics and dynamics of confined RTIL solutions, we proceeded by performing two kinds of independent simulation experiments: (i) on one hand, we undertook pore-like simulations (hereafter referred to as experiments of type $\mathcal{P}$) comprising RTIL solutions, with IL global concentrations and water molar fractions taken from these previous experiments, confined within $l = 66$ Å, longer tubular pores, periodically replicated along the z-direction; (ii) on the other hand, and as reference systems, we also performed standard, bulk-like, simulations experiments (hereafter referred to as type $\mathcal{B}$) of fully periodic aqueous solutions of RTILs, with concentrations and water molar fractions taken from c_{IL}^{blk} and x_{IL}^{blk}, respectively.

The analysis of results from experiments of type $\mathcal{P}$ showed that the interiors of the pores also represent inhomogeneous environments for the ionic solvation. In Figure 4 we present results for $\rho_{rad}^\alpha(r)$, the distributions along the radial direction of the different species, namely

$$\rho_\alpha^{rad}(r) = \frac{1}{2\pi r L_z} \sum_i \langle \delta(r_i^\alpha - r) \rangle_{\mathcal{P}} \quad (3)$$

where r_i^α represents the distance of the ith particle of species α to the axis of the pore and $\langle ... \rangle_{\mathcal{P}}$ represents averages collected along experiments of type $\mathcal{P}$.

Similarly to what we have found in the results for $\rho_\alpha^z(z)$, for both RTILs, the most prominent fluctuations are those observed for the $[BMIM]^+$ species, which remain tightly adsorbed to the wall of the hydrophobic pores (see the peaks at

dx.doi.org/10.1021/jp211101a | J. Phys. Chem. C 2012, 116, 5394−5400

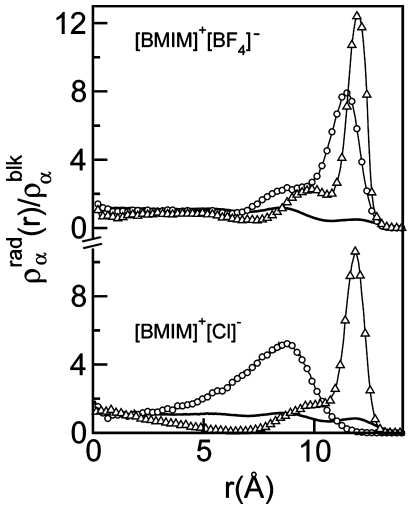

Figure 4. Normalized radial density fields for different species of confined RTILs within hydrophobic pores of radius R = 12.5 Å at T = 323 K. Water, solid line; cations, triangles; anions, circles.

$r \sim 12$ Å). As we move to shorter radii, the profiles exhibit shoulder-like structures at $r \sim 9-10$ Å, followed by an intermediate, 5 Å $\lesssim r \lesssim$ 8 Å, inner region practically deprived of $[BMIM]^+$ ions. Finally, one arrives to the central region, where the local concentrations attain practically bulk values.

To gain additional insight about the nature of wall-solvation states of the $[BMIM]^+$ ions, we also computed local orientational correlations of the imidazolium rings with respect to the r direction, in terms of the angles

$$\cos\theta_i = \hat{\mathbf{n}}_i \cdot \hat{\mathbf{r}} \tag{4}$$

In the previous equation, $\hat{\mathbf{n}}_i$ represents a unit vector perpendicular to the i-th imidazolium ring and $\hat{\mathbf{r}}$ a unit vector along the r direction. More specifically, we focused attention on distributions of the type

$$\overline{P_2(\cos\theta)}(r) = \frac{1}{N_r} \sum_{i=1}^{N_r}{}' P_2(\cos\theta_i) \tag{5}$$

where $P_2(x) = (3x^2 - 1)/2$ and the prime denotes a sum restricted to $[BMIM]^+$ cations which lie in a Δr = 0.5 Å interval, centered at r, containing N_r molecules. The results appear in Figure.5. In both RTILs, the profiles for $\overline{P_2(\cos\theta)}(r)$ suggest that wall-solvation states are characterized by cations with their ring planes parallel to the interface, i.e., cos $\theta_i \sim 1$. Moreover, the plots also show a secondary preferential orientation $\theta_i \sim 60°$ for those cations lying at the 8 Å $\lesssim r \lesssim$ 10 Å inner interval and a complete loss of orientational correlation for the rest of the groups, localized at the center of the pore.

The normalized distributions of the anions in Figure 4 present distinctive features: (i) on one hand, the plot for Cl^- presents a broad peak of magnitude ∼5, adjacent and practically segregated from the $[BMIM]^+$ one. The peak spans the 5 Å $\lesssim r \lesssim$ 10 Å, more central region of the pore and reveals the absence of wall-solvation states for these species; (ii) on the other hand, the plot corresponding to the more hydrophobic $[BF_4]^-$ anions is dominated by a peak of magnitude ∼8, centered at r = 11.5 Å that would be compatible with, at least, partial wall-like solvation. As we will see in the next section, these structural differences, i.e., adjacent-segregated vs partially overlapped-wall solvation structures, might be indicative of modifications in the mechanisms that control transport properties in the two RTIL solutions that we investigated.

B. Dynamical Analysis. Our dynamical analysis will be focused on the examination of mass and charge transport coefficients along the axial direction of the pore. In particular, individual diffusion coefficients, $D_\alpha^{\parallel}$, were computed from the limiting slopes of $\mathcal{R}_\alpha^2$, the root-mean-square displacements, namely

$$D_\alpha^{\parallel} = \lim_{t\to\infty} \frac{\mathcal{R}_\alpha^2}{2t} = \lim_{t\to\infty} \frac{\langle |z_\alpha^i(t) - z_\alpha^i(0)|^2 \rangle_{\mathcal{P}}}{2t} \tag{6}$$

Results for $\mathcal{R}_\alpha^2(t)$ for water and the ionic species are depicted in Figure 6, whereas results for $D_\alpha^{\parallel}$ are listed in Table 1a. At a first glance, the plots reveal that the root mean displacements of the confined ions remain in the sublinear temporal regime over time spans unusually long for standard liquid phases. Yet, these time scales are those required for the different species to travel distances comparable to their molecular sizes. For the particular case of adsorbed $[BMIM]^+$ groups, even after 1 ns, the linear regime seems to be only marginally satisfied. Given the characteristics of the wall-solvation already described, we cannot discard that this sublineal temporal regime might reflect the presence of mechanisms akin to highly correlated "single-file-diffusion" motions, in which surpassing episodes between different particles are severely hindered.

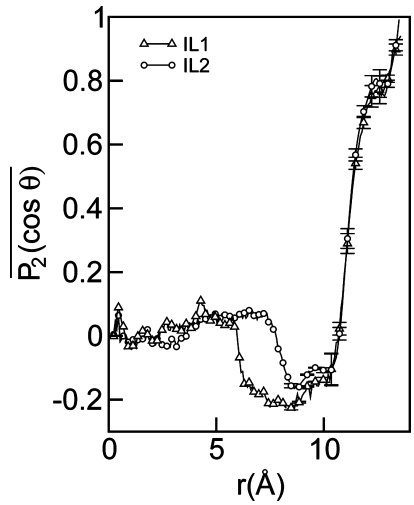

Figure 5. Local orientational correlations for the imidazolium rings of $[BMIM]^+$ groups along the radial direction for confined RTILs, within hydrophobic pores of radius R = 12.5 Å at T = 323 K. The error bars correspond to standard deviations taken from five statistically independent, 20 ns trajectories (see text). For clarity purposes, error bars are restricted to the r > 8 Å interval.

In Table 1b, we have included reference bulk results from simulations of type $\mathcal{B}$. As we mentioned before, despite the approximations involved in neglecting polarization fluctuations in our model Hamiltonian, simulation predictions compare experimental data.[49] Confinement promotes a drop in the diffusion coefficients of water and $[Cl]^-$ by a factor of ∼2. Modifications in the transport of bulkier and more hydrophobic ions are much more dramatic: upon confinement, the diffusion coefficient of $[BF_4]^-$ drops a factor of ∼7−8, whereas the ones for $[BMIM]^+$ get reduced by up to a factor of ∼20. Note that

dx.doi.org/10.1021/jp211101a | J. Phys. Chem. C 2012, 116, 5394−5400

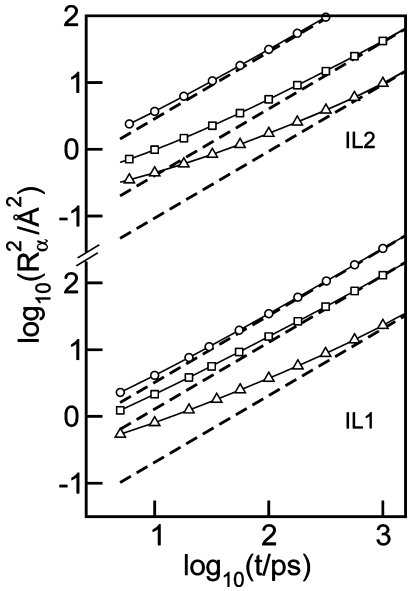

Figure 6. Root mean square displacements for different species comprising confined RTIL solutions within hydrophobic pores of radius R = 12.5 Å at T = 323 K. Water, circles; anions, squares; cations, triangles. The dashed lines correspond to asymptotic linear plots, with slope one.

these modifications in the transport correlate reasonably well with the magnitude of the structural modifications operated in the local density fields described in the previous section. More interestingly, these effects seem to be also controlled, to some extent, by the presence of nearby bulkier anions which—as in the case of heavier $[BF_4]^-$ groups—may reinforce the retardation effects imposed by the presence of a nearby static, solid interface.

The analysis of the charge transport in terms of the time correlation function of the parallel current provides additional insights into the mechanisms that control the translational modes of the confined RTILs. In the sixth column of Table 1, we present results for $\sigma^{\parallel}$, the ionic conductivity, computed from the time correlation function of $J^{\parallel}$, namely[50]

$$\sigma^{\parallel} = \frac{1}{k_B TV}\int_0^{\infty} \langle J^{\parallel}(t)\cdot J^{\parallel}(0)\rangle_{\mathcal{P}} \mathrm{d}t$$
$$J^{\parallel}(t) = \sum_{i,\alpha} Z_{\alpha} e\, \dot{z}_{\alpha}^{i}(t) \tag{7}$$

where V represents the volume of the pore; k_B is the Boltzmann constant; and $Z_\alpha e$ is the charge of species α. The direct comparison between confined and bulk results for $\sigma^{\parallel}$ does not allow us to establish conclusive trends, in particular because, quite unexpectedly, the ionic conductivity for confined IL1 solutions was found to be greater than the one recorded in the bulk.

In principle, one could be tempted to invoke a delicate balance between the increment in the number of charge carriers within the pores and the retardations observed in the translational modes to account for the variations in $\sigma^{\parallel}$. Although this is true, we will shortly show that additional effects will also need to be considered. To move forward in our analysis, it will be useful to perform the standard decomposition of the expression of the conductivity, namely[50]

$$\sigma^{\parallel} = \sigma^{\parallel}_{\mathrm{NE}}(1 + \Delta) \tag{8}$$

where $\sigma^{\parallel}$ represents the so-called Nerst−Einstein (NE) approximation. For an $[M]^+[X]^-$ aqueous solution containing N ion pairs, the expression for σ_{NE} is

$$\sigma^{\parallel}_{\mathrm{NE}} = \frac{Ne^2}{k_B TV}(D^{\parallel}_{M^+} + D^{\parallel}_{X^-}) \tag{9}$$

As such, the NE expression neglects contributions from cross-dynamical correlations between pairs of particles which, in turn, are included in the Δ term.

Usually, Δ is a negative quantity; in other words, the incorporation of correlations between velocities of different particles leads to an overall reduction in the electrical conductivity. While this feature holds for pure RTILs[51] and for aqueous solutions as well (see entries in column 7 of Table 1b), the simulation results listed in Table 1a reveal that this characteristic is not satisfied in confined solutions. We remark that such positive deviations have also been reported in molten salts comprising noble-metal halides.[52−55]

Looking for clues to rationalize this peculiarity, we further decomposed the expression of Δ into contributions from three distinct, cross-diffusion coefficients of the type

$$\Delta = \Delta_{M^+M^+} + \Delta_{X^+X^-} - 2\Delta_{M^+X^-} = \frac{D^{d}_{M^+M^+} + D^{d}_{X^-X^-} - 2D^{d}_{M^+X^-}}{D^{\parallel}_{M^+} + D^{\parallel}_{X^-}}$$
$$D^{d}_{\alpha\gamma} = N\int_0^{\infty} \langle \dot{z}^{i}_{\alpha}(0)\cdot \dot{z}^{j}_{\gamma}(t)\rangle \mathrm{d}t \tag{10}$$

Results for $\Delta_{\alpha\gamma}$ (α = M^+, X^-) are listed in the last three columns of Table 1. In IL1, the largest contribution to the Δ term comes from cross-correlations between $[Cl]^-$−$[Cl]^-$ pairs (which are the fastest), whereas in the IL2 solution, the contributions from the three cross-terms are much more comparable. As a result, deviations from the NE behavior are

Table 1. Transport Coefficients for Confined and Bulk Ionic Liquid−Water Solutions at T = 323 K

RTIL	c	$D^{\parallel}_{W}$	$D^{\parallel}_{X^-}$	$D^{\parallel}_{M^+}$	$\sigma^{\parallel}$				
$[M]^+[X]^-$	M		10^{-5} cm^2 s^{-1}		Ω^{-1} m^{-1}	Δ	$\Delta_{X^-X^-}$	$\Delta_{M^+M^+}$	$\Delta_{X^-M^+}$
a. Pore results[a]									
$[BMIM]^+[Cl]^-$	2.1	1.7	0.67	0.13	9.6	0.67	1.2	0.17	0.35
$[BMIM]^+[BF_4]^-$	2.9	1.4	0.21	0.046	3.3	0.29	0.65	0.17	0.27
b. Bulk results[b]									
$[BMIM]^+[Cl]^-$	0.87	2.8	1.4	0.96	6.5	−0.07	−0.03	−0.03	0.004
$[BMIM]^+[BF_4]^-$	0.77	2.8	1.7	1.0	5.4	−0.24	−0.14	−0.08	0.008

[a]Results from experiments of type $\mathcal{P}$ (see text). [b]Results from experiments of type $\mathcal{B}$ (see text).

dx.doi.org/10.1021/jp211101a | J. Phys. Chem. C 2012, 116, 5394−5400

somewhat more marked in the IL1—about ∼70%—than in the IL2 case, ∼25%.

The physical interpretation of these changes is not always straightforward. Still, in the present context, one could speculate that some clues could be obtained from the simple consideration of the differences in the spatial correlations of the different species within the pore shown in Figure 4. More specifically, in IL1 solutions, we recall that the gross features of $\rho_\alpha^{rad}(r)$ can be cast in terms of the segregation of the two ionic species within adjacent, coaxial sections. As such, correlated motions between pairs of ions with the same charge should prevail upon those involving neutral, $[Cl]^-[BMIM]^+$, pairs. Contrasting, in IL2 solutions, the overlap between the $\rho_\alpha^{rad}(r)$ distributions would indicate a larger extent of cancellations between the different $\Delta_{\alpha\gamma}$, leading to a smaller, albeit still positive, value of Δ. Incidentally, similar connections between segregation and transport within nanocavities have been established in a recent analysis of cross fluxes of mixtures of protic−aprotic solvents.[56]

IV. CONCLUDING REMARKS

The results presented in this paper shed light on new features related to structural and dynamical characteristics of aqueous solutions of RTILs, confined within hydrophobic cylindrical pores of nanometric dimensions. We start by pointing out that the presence of a hydrophobic, solid-like substrate promotes enhancements of the local densities of bulky ionic groups—such as $[BMIM]^+$ and $[BF_4]^-$—at its close vicinity. Such segregation is akin to the concentration fluctuations of large groups reported at liquid−air interfaces in RTIL−water solutions.[24] Within a more general framework, the phenomenon could also be ascribed to the well-documented tendency of water to stay away from large hydrophobic-like solutes.[57] Although the concept of "hydrophobicity" applied to groups such as $[BMIM]^+$ or $[BF_4]^-$ may still be subjected to a certain extent of ambiguity, in the present context, we are referring to groups with two distinctive characteristics: (i) a molecular size well beyond the one of a water molecule and (ii) an overall weak Coulomb coupling with the aqueous environment, due also to the large length scales characterizing their corresponding charge distributions.

Our results reveal a preferential wall adsorption of $[BMIM]^+$ groups and a somewhat more attenuated propensity for $[BF_4]^-$ anionic species. Moreover, the solvation of the former groups is characterized by strong orientational correlations of their imidazolium groups, which remain practically parallel to the pore walls. To preserve electroneutrality, the excess of the positive charge at the interface goes hand in hand with local increments of the concentrations of the corresponding counterions. As a result, these modifications lead to overall concentrations of the ionic species which, for pores with $R \sim 1-2$ nm, are between 2 and 3 times larger than the ones prevailing in bulk regions.

In passing, we remark that this structural description contrasts sharply to the complementary one found in simpler confined aqueous electrolytes, where the first solvation shells of each individual ion are preserved and the ionic species are segregated away from the walls, into the central, "bulk-like", region of the pores. As such, the presence of an outer aqueous shell deprived from ionic species leads to a net depletion of global pore salt concentration. Interestingly, the scenario in IL1 solutions could be pictured as a "hybrid" one, characterized by $[BMIM]^+$ groups exhibiting wall-like solvation states and $[Cl]^-$ ions lying at inner regions of the pore, segregated from the more external shell occupied by the $[BMIM]^+$ groups.

Concerning transport properties, the localization of a sizable fraction of the ionic species in outer regions of the pore brings down pore diffusion coefficients by a factor of ∼0.5 for the fastest $[Cl]^-$ ions. For bulkier groups such as $[BMIM]^+$ and $[BF_4]^-$, the drop may go down by practically 2 orders of magnitude. Modifications in $\sigma^{\parallel}$ are not uniform and seem to be a result of a complex interplay in which intervene, at least, three competing effects from: (i) the already mentioned retardations of the diffusive motions; (ii) the net increment in the concentrations of charge carriers within the pore; and (iii) cross-dynamical correlations, which would be dictated, in part, by the characteristics of the different local ionic densities within the pores. In IL1 solutions, the combined effects (ii) and (iii) would prevail upon the retardations. By "dissecting" the Δ term into its three contributions $\Delta_{\alpha\gamma}$, we found that the overall effects of cross dynamical correlations are dominated by contributions from velocities of nearby $[Cl]^-$−$[Cl]^-$ pairs that would be positively correlated. This behavior would clash with the one observed in pure and aqueous solutions of binary RTILs, where cation−cation and anion−anion distinctive diffusive coefficients are usually negative. As a plausible argument to account for these differences, we tend to believe that the segregation of $[Cl]^-$ and $[BMIM]^+$ groups in adjacent, concentrical shells with boundaries perpendicular to the z-direction could reinforce cooperative effects between the equally charged ions. As an additional element to support this line of reasoning, we remark that, in IL2 solutions, the larger overlap between ρ_{BMIM}^{rad} and $\rho_{BF_4}^{rad}$ at the outer, $r \gtrsim 10$ Å, region would render the three distinctive diffusion coefficients much more comparable in size, bringing down the value of Δ.

Although additional experiments oriented to the identification of microscopic mechanisms controlling mass and charge transport in pores are surely called for, we believe that this first physical interpretation based on the characteristics of the segregations of the ionic species is physically sound. As such, the simulation results described in this paper represent a body of new and interesting behaviors concerning structural and dynamical characteristics of confined RTIL aqueous solutions that differ at a qualitative level not only from those found in bulk phases but also from those observed in simpler aqueous electrolytes under similar conditions of confinement. A deeper analysis based on the time characteristics of the different cross correlation functions is currently underway in our laboratory.

AUTHOR INFORMATION

Corresponding Author

*Email: dhlaria@cnea.gov.ar.

Notes

The authors declare no competing financial interest.

ACKNOWLEDGMENTS

JR, MDE, and DL are staff members of CONICET, Argentina.

REFERENCES

(1) Anthony, J. L.; Maginn, E. J.; Brennecke, J. F. *J. Phys. Chem. B* **2001**, *105*, 10942−19049.

(2) Takamuku, T.; Kyoshoin, Y.; Shimonura, T.; Kittaka, S.; Yamaguchi, T. *J. Phys. Chem. B* **2009**, *113*, 10817−10824.

(3) Méndez-Morales, T.; Carrete, J.; Cabeza, O.; Gallego, L. J.; Varela, L. M. *J. Phys. Chem. B* **2011**, *115*, 6995−7008.

(4) Cammarata, L.; Kazarian, S. G.; Salter, P. A.; Welton, T. *Phys. Chem. Chem. Phys.* **2001**, *3*, 5192−5200.
(5) Hanke, C. G.; Lynden-Bell, R. M. *J. Phys. Chem. B* **2003**, *107*, 10873−10878.
(6) Sun, B.; Jin, Q.; Tan, L.; Wu, P.; Yan, F. *J. Phys. Chem. B* **2008**, *112*, 14251−14259.
(7) Spickermann, C.; Thar, J.; Lehmann, S. B. C.; Zahn, S.; Hunger, J.; Buchner, R.; Hunt, P. A.; Welton, T.; Kirchner, B. *J. Chem. Phys.* **2008**, *129*, 104505.
(8) Moreno, M.; Catiglione, F.; Mele, A.; Pasqui, C.; Raos, G. *J. Phys. Chem. B* **2008**, *112*, 7826−7836.
(9) Wang, H.; Wang, J.; Zhang, S.; Xuan, X. *J. Phys. Chem. B* **2008**, *112*, 16682−16689.
(10) Schröder, G.; Neumayr, G.; Steinhauser, O. *J. Chem. Phys.* **2009**, *130*, 194503.
(11) Jian, W.; Wang, Y.; Voth, G. A. *J. Phys. Chem. B* **2007**, *111*, 4812−4818.
(12) Feng, S.; Voth, G. A. *Fluid Phase Equilib.* **2010**, *294*, 148−156.
(13) Bhargava, B. L.; Klein, M. L. *J. Phys. Chem. B* **2009**, *113*, 9499−9505.
(14) Łuczak, J.; Hupka, H.; Thöming, J.; Jungnickel, C. *Colloids Surf., A* **2008**, *329*, 125−133.
(15) Singh, T.; Kumar, A. *J. Phys. Chem. B* **2007**, *111*, 7843−7851.
(16) Dong, B.; Zhao, X.; Zheng, L.; Zhang, J.; Li, N.; Ionue, T. *Colloids Surf., A* **2008**, *317*, 666−672.
(17) Du, F-. Y.; Xiao, X-. H.; Li, G-. K. *J. Chromatogr. A* **2007**, *1140*, 56−62.
(18) Huddleston, J. G.; Willauer, H. D.; Swatloski, R. P.; Visser, A. E.; Rogers, R. D. *Chem. Commun.* **1998**, *44*, 1765−1766.
(19) Zhao, X.; Gu, Y.; Li, J.; Ding, H.; Shan, Y. *Catal. Commun.* **2008**, *9*, 2179−2182.
(20) Yokozeki, A.; Shiflett, M. B. *Ind. Eng. Chem. Res.* **2010**, *49*, 9496−9503.
(21) Chaumont, A.; Schurhammer, R.; Wipff, G. *J. Phys. Chem. B* **2005**, *109*, 18964−18973.
(22) Chevrot, G.; Schurhammer, R.; Wipff, G. *Phys. Chem. Chem. Phys.* **2006**, *8*, 4166−4174.
(23) Lynden-Bell, R. M.; Del Pópolo, M. *Phys. Chem. Chem. Phys.* **2006**, *8*, 949−954.
(24) Picálek, J.; Minofar, B.; Kolafa, J.; Jungwirth, P. *Phys. Chem. Chem. Phys.* **2008**, *10*, 5765−5775.
(25) Rivera-Rubero, S.; Baldelli, S. *J. Am. Chem. Soc.* **2004**, *126*, 11788−11789.
(26) Baldelli, S. *J. Phys. Chem. B* **2003**, *107*, 6148−6152.
(27) Rivera-Rubero, S.; Baldelli, S. *J. Phys. Chem. B* **2006**, *110*, 15499−15505.
(28) Gómez, E.; González, B.; Domínguez, A.; Tojo, E.; Tojo, J. *J. Chem. Eng. Data* **2006**, *51*, 696−701.
(29) English, N. J.; Mooney, D. A.; O'Brien, S. W. *J. Mol. Liq.* **2010**, *157*, 163−167.
(30) Gu, Y.; Ogawa, C.; Mori, J.; Kobayashi, S. *Angew. Chem., Int. Ed.* **2006**, *45*, 7217−2220.
(31) Gu, Y.; Ogawa, C.; Kobayashi, S. *Org. Lett.* **2007**, *9*, 175−178.
(32) Pinilla, C.; Del Pópolo, M. G.; Lynden-Bell, R. M.; Kohanoff, J. *J. Chem. Phys. B* **2005**, *109*, 17922−17927.
(33) Pinilla, C.; Del Pópolo, M. G.; Kohanoff, J.; Lynden-Bell, R. M. *J. Phys. Chem. B* **2007**, *111*, 4877−4884.
(34) Singh, M. P.; Singh, R. K.; Chandra, S. *J. Phys. Chem. B* **2011**, *115*, 7505−7514.
(35) Coasne, B.; Viau, L.; Voux, A. *J. Phys. Chem. Lett.* **2011**, *2*, 1150−1154.
(36) Iacob, C.; Sangoro, J. R.; Papadopoulos, P.; Schuber, T.; Naumov, S.; Valiullin, R.; Kärger, J.; Kremer, F. *Phys. Chem. Chem. Phys.* **2010**, *12*, 13798−13803.
(37) Videla, P. E.; Sala, J.; Martí, J.; Guàrdia, E.; Laria, D. *J. Chem. Phys.* **2011**, *135*, 104503.
(38) Morales, C. M.; Thompson, W. H. *J. Phys. Chem. A* **2009**, *113*, 1922−1933.
(39) Gulmen, T. S.; Thompson, W. H. *Mater. Res. Soc. Symp. Proc.* **889E** 0899-N06−05.1.10 (**2006**).
(40) Yang, Q.; Zhang, H.; Su, B.; Yang, Y.; Ren, Q.; Xing, H. *J. Chem. Eng. Data* **2010**, *55*, 1745−1749.
(41) Zhou, Q.; Wang, L.-S. *J. Chem. Eng. Data* **2006**, *51*, 905−908.
(42) Phillips, J. C.; Braun, R.; Wang, W.; Gumbart, J.; Tajkhorshid, E.; Villa, E.; Chipot, C.; Skeel, R. D.; Kale, L.; Schulten, K. *J. Comput. Chem.* **2005**, *26*, 1781−1802.
(43) Berendsen, H. J. C.; Grigera, J. R.; Straatsma, T. P. *J. Phys. Chem.* **1987**, *91*, 6269−6271.
(44) Liu, Z.; Huang, S.; Wang, W. *J. Phys. Chem. B* **2004**, *108*, 12978−12989.
(45) Siqueira, L. J. A.; Ribeiro, M. C. C. *J. Phys. Chem. B* **2007**, *111*, 11776−11785.
(46) Lynden-Bell, R. M.; Youngs, T. G. A. *J. Phys.: Condens. Matter* **2009**, *21*, 424120.
(47) Liu, Z. P.; Chen, T.; Bell, A.; Smit, B. *J. Phys. Chem. B* **2010**, *114*, 4572−4582.
(48) Essmann, U.; Perera, L.; Berkowitz, M. L.; Darden, T.; Lee, H.; Pedersen, L. G. *J. Chem. Phys.* **1995**, *103*, 8577−8593.
(49) For experimental information of transport coefficients in RTIL−water mixtures, see, for example: Sarraute, S.; Costa Gomes, M. F.; Pádua, A. A. H. *J. Chem. Eng. Data* **2009**, *54*, 2389−2394. Rilo, E.; Vila, J.; Pico, J.; García-Garabal, S.; Segade, L.; Varela, L. M.; Cabeza, O. *J. Chem. Eng. Data* **2010**, *55*, 639−644.
(50) See, for example : Hansen, J-. P.; McDonald, I. *Theory of simple Liquids*; Academic Press: Amsterdam, 2006; Chapter 10.
(51) Kashyap, H. K.; Annapureddy, H. V. R.; Raineri, F. O.; Margulis, C. J. *J. Phys. Chem. B* **2011**, *115*, 13212−13221.
(52) Trullàs, J.; Padró, J. A. *Phys. Rev. B* **1997**, *55*, 12210−12217.
(53) Trullàs, J.; Alcaraz, O.; González, L. E.; Silbert, M. *J. Phys. Chem. B* **2003**, *107*, 282−290.
(54) Tasseven, C.; Trullàs, J.; Alcaraz, O.; Silbert, M.; Giró, A. *J. Chem. Phys.* **1997**, *106*, 7286−7294.
(55) Yamaguchi, T.; Nagao, A.; Matsuoka, T.; Koda, S. *J. Chem. Phys.* **2003**, *119*, 11306−11317.
(56) Rodriguez, J.; Elola, M. D.; Laria, D. *J. Phys. Chem. B* **2009**, *113*, 12744−12749.
(57) See, for example: Chandler, D. *Nature* **2005**, *437*, 640−647.